Design and Characterization of an Adamantane Thruster for Cubesat Applications

IEPC-2024-163

Presented at the 38th International Electric Propulsion Conference
Pierre Baudis Convention Center • Toulouse, France
June 23-28, 2024

Olivia Kukar[1], Kayden Elmer-Schurr[1], Kayden Cutchins[1], Jonathan Fisher[1], Emily Lo[1], Cameron Coen[1], Autumn Zaretsky[1], Max Wu[2], Lubos Brieda[3], and Matthew Gilpin[4]
University of Southern California, Viterbi School of Engineering, Los Angeles, CA, 90007, USA

Abstract: The Advanced Spacecraft Propulsion and Energy (ASPEN) Lab at the University of Southern California has started developing and characterizing a plasma thruster operating on solid propellant adamantane ($C_{10}H_{16}$). The thruster is envisioned to operate in a "solid rocket" mode, with each thruster head delivering a finite amount of delta-V after activation and operating until propellant depletion. The use of a solid propellant alleviates the need to include high-pressure tanks and the related plumbing. The thruster has been demonstrated to operate at low power levels available on Cubesats, with thrust measured using a laser-based system. In this paper, we describe the additional optimization, including the use of a 3D-printed miniature thruster body, experimental characterization of plume properties through a constructed Langmuir probe, two-dimensional plume simulations, as well as molecular dynamics simulations of fragmentation. Current measurements show high promise of adamantane being a viable propellant source in deorbiting CubeSats due to its compact, simplistic design and comparable ISP to similar systems.

I. Motivation and Background

The demand for effective deorbiting systems has surged in response to the Federal Communications Commission's new regulations mandating low-Earth orbit satellites to deorbit within five years post-mission completion. This regulatory change has spurred interest in developing electric propulsion systems that are feasible within the constrained power, mass, and volume budgets of CubeSats and other similar nanosatellites. Although gridded ion and Hall effect thrusters have been widely adopted for stationkeeping and orbital adjustments in telecommunications constellations and scientific missions, scaling these devices down to suit the limited size and power capabilities of CubeSats presents significant challenges.[1] Many require pressurized vessels to store gaseous propellants like Xenon. These are volume-intensive, and require significant plumbing complexity and miniaturization of components.[2]

To address these challenges, the Advanced Spacecraft Propulsion and Energy (ASPEN) Laboratory at the University of Southern California is pioneering the development of a plasma thruster that utilizes solid adamantane ($C_{10}H_{16}$) as the propellant. Adamantane's solid crystalline state at room temperature and its ability to directly sublimate at a reasonable vapor pressure without heaters or a catalyst makes it an attractive propellant for a low-complexity system. Self-pressurizing solid propellant reduces hardware complexity, mass, and volume eliminating the need for heaters or pressurized storage, and the proof of concept testing presented here shows that

1 Undergraduate Student, Viterbi School of Engineering, okukar@usc.edu, elmersch@usc.edu, kcutchin@usc.edu, fisherjr@usc.edu, eflo@usc.edu, ccoen@usc.edu, azartsk@usc.edu

2 Undergraduate Student, Dornsife School of Arts and Sciences, mxwu@usc.edu

3 Part-time Lecturer of Astronautical Engineering, Viterbi School of Engineering, brieda@usc.edu.

4 Associate Professor of Aerospace and Mechanical Engineering Practice, Viterbi School of Engineering, gilpin@usc.edu

sublimated adamantane can be directly ionized for use as a propellant. It is proposed that an adamantane-based low-complexity plasma thruster system can be developed as a single-use de-orbit thruster where a fixed amount of pre-loaded propellant is allowed to flow through the thruster after breaking a seal that separates solid adamantane from the thruster body. A single-use design eliminates the need for complex valves or regulators, replacing them with a simple membrane that can be broken to deliver the full ΔV when needed. Such a system would result in a significant reduction in dry mass through relatively high Isp operation of a plasma thruster with low power requirements and low system volume.

This paper proposes the design and operation of this propulsion device along with notes on preliminary experimental development and modeling. ASPEN is an undergraduate student-led organization at the University of Southern California and has recently begun developing capabilities for the design and testing of electric propulsion concepts. The lab's current goal is to validate adamantane as a potential solid fuel for the proposed CubeSat deorbit propulsion system. This paper discusses comparisons of an adamantane-based system against other CubeSat scale propulsion devices and then discusses the overall design of a prototype thruster. Initial experimental and modeling results are also discussed demonstrating initial thruster measurements and the use of sublimated adamantane as a viable propellant. Finally, the paper presents a comparative analysis of experimental findings and simulation outcomes, offering a comprehensive understanding of the thruster's performance. Throughout this process, the ASPEN Laboratory has used the development of this thruster to establish a viable propulsion testing and development facility with the necessary hardware and diagnostics to support the future development and miniaturization of an adamantane-based de-orbit system.

II. Thruster Design

An adamantane-based propulsion system is proposed with an emphasis on simplicity to reduce mass, volume, and power requirements with the ultimate goal of creating a miniaturized propulsion unit specifically designed to deliver the required ΔV for de-orbit. A simple test thruster has been built to demonstrate ionization of adamantane and thruster generation and development work is ongoing for the implementation of key thruster components. Specifically, this thruster concept relies on an easily breakable membrane that can contain solid propellant before the desired operation.

A. Basic Thruster Concept

Fig. 1 shows a representative diagram of the proposed thruster. As a propellant, Adamantane does not require an external pressurized propellant tank, the additional piping and control systems to transfer propellant from this propellant tank, or a heating element to sublimate. The solid propellant is stored in the same vicinity as the ionization chamber with only a small valve/membrane enclosing the solid adamantane until thruster operation is desired. By using a single-use design, the propellant storage system for this thruster is simpler than other small-satellite systems while maintaining relatively high ISP operation. The advantages of the proposed system can be highlighted by comparing the proposed system to current COTS CubeSat scale propulsion devices such as the VACCO's MiPS cold gas system which requires a complete system for propellant storage, pressurization, and distribution. VACCO's system has a wet mass of 542g and takes up a .3U.[3] Adamantane's benefit in simplicity and high density allows for distinct reductions in the overall propellant system mass. To highlight this, consider a comparison to a current COTS warm gas CubeSat thruster, the VACCO MiPS. If we were to operate at the same Isp of ~40-100s (which is likely a significant underestimate as theoretical Isp is 300-400s), as discussed in Section II B, the overall volume of adamantane required for the same delta V requires ~.2U, in comparison to the .3U required for the MiPS propellant. Assuming we can operate at a similar Isp (~40-100s), our solid-fuel adamantane system could reduce the overall mass and volume of this system by at least 100 grams and 0.1U simply by eliminating the need for additional propellant distribution and pressurization equipment.[3]

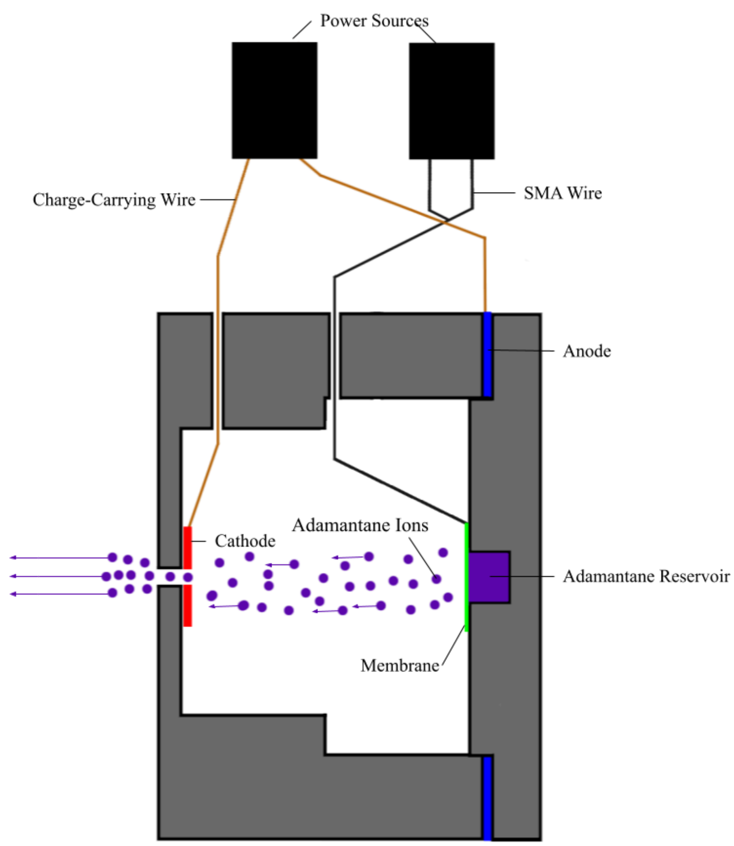

Figure 1. Schematic diagram of the proposed adamantane-based plasma thruster. Solid propellant is stored in the reservoir and allowed to sublimate into the thruster body, where it is ionized and accelerated through an orifice.

An additional benefit of the proposed thruster is low steady-state power requirements which is compatible with the low power available on micro and nanosatellites. Typically, microsatellites operate with a total power budget of approximately 5-20W.[5] Current marketable micro satellite propulsion systems struggled most with reducing their maximum Steady-State Power and required Stand-By Power to meet those requirements. For example, Benchmark Space System's Starling CubeSat warm gas thruster requires 10 W for pressurization, 15-50 W to operate its resistojet, and up to 3 W for its thrust valve.[6] Thus, our goal is to develop a system that can ultimately operate under 2 W of steady-state power, allowing for continuous operation on a CubeSat platform. Our system operates at high voltage and low current, giving us more room to reduce our wattage requirements. In addition, our simplistic design reduces the need for additional power to operate pressurization systems and heating elements. Further studies will explore the best way to minimize the power draw from the supply and ensure our high voltage requirements are met.

B. Current Thruster Hardware

A simple thruster has been designed to confirm adamantane's ability to serve as a propellant. As such, simplicity and ease of construction were prioritized for rapid iteration and low-cost manufacturing. This also ensured that minor adjustments could be quickly carried out and that the design would be capable of being reduced in scale for future integration on CubeSat platforms. Additionally, given the limited resources available to ASPEN, the thruster was 3D printed from a clear resin for easy viewing while still maintaining functionality under low-pressure environments.

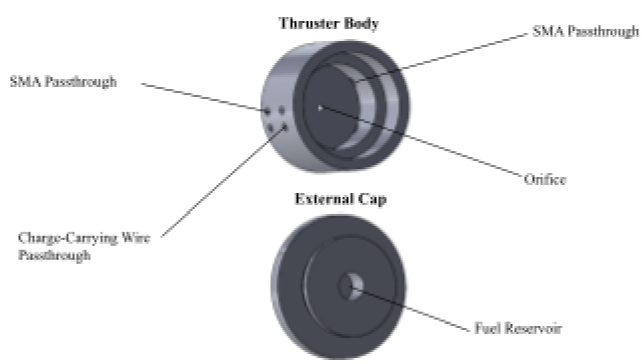

Figure 2. Drawing of the current thruster test article consisting of two 3D printed halves. The removable external cap allows for easy propellant reloading in the fuel reservoir and access to install the anode, cathode, and prototype SMA-based membrane separation system.

The thruster body is composed of a cylinder approximately 12.7 mm in length and 23 mm in diameter with one circular face open and the other closed. Within the center of the closed end, an orifice is created nominally 0.5 mm in diameter for ions to be ejected through. Along the wall of the main body are two pairs of holes, allowing a loop of conductive wire and a loop of shape memory alloy (SMA) wire to pass into the thruster body. Furthermore, the thruster features an external cap to fit over the open end of the main body, in which a small secondary reservoir is milled to store propellant within. A conductive ring is placed within the thruster, while another is fixed between the thruster body's recess and the external cap. The conductive wire is then attached to both the conductive discs, charging them to create an electric field directed towards the orifice.

Furthermore, an impermeable membrane can then be placed over the reservoir within the external cap to maintain pressurization of the propellant during pump down. Once the testing chamber is at the desired pressure, the membrane can be removed to allow sublimation of the adamantane. The primary method investigated was to attach the SMA wire to the membrane through the dedicated passthrough. The construction of this membrane will be further addressed later in this paper.

C. Membrane/Valve Construction

It is necessary to implement a mechanism to ensure that stored propellant does not sublimate before the thruster is required while in orbit. Though the development of this mechanism is still ongoing, the primary method under investigation was the implementation of a breakable membrane sealing the propellant chamber, before being removed or broken upon firing of the thruster.

A series of potential membrane materials must be evaluated and demonstrate a solution that can be reliably broken or removed after pumping down to release the sublimated propellant into the ionization chamber. This material must operate with a low power requirement and with a minimized geometry to maximize the neutral gas entering into the ionization chamber without bouncing back into the propellant chamber. When exploring possible materials, it is important to note the outgassing properties of the material, their response to high temperatures, and their reproducibility. With the lack of a wet laboratory, all materials explored were pre-manufactured.

To begin, a thin polypropylene film was secured with o-ring seals between the propellant chamber and the ionization chamber. A shape memory alloy wire (SMA) was then secured in the chamber and pressed against the membrane. When the SMA was heated, it would then straighten and tear the polypropylene film, allowing the propellant to flow into the ionization chamber. Preliminary tests showed difficulty in tearing the polypropylene film with moderately sized SMA wires (.75-1 mm in diameter). To reliably pierce the membrane, an SMA wire with a higher temperature rating and diameter of 1-1.5 mm was required and testing showed inconsistent results. Minute adjustments to the geometry changed whether the membrane tore and if so the tear was not uniform.

Experimentation then deviated from a thin film to a solid disk with an embedded SMA. Epoxy cast and plaster were tested. Although these materials did include high off-gassing properties, they were readily available materials that mimicked more viable materials such as acrylic. These materials were set in a simple circular mold with a diameter of one inch that allowed the SMA to be embedded around the exterior of the circle. The mold was made thinner towards the center to include targeted weak points allowing the SMA to break the disk. Testing showed difficulty in embedding the SMA wire. The primary difficulty was encountered when attempting to properly bend the wire to fit in the mold and illustrated more geometry challenges in securing the wire at difficult angles within the small size of the thruster.

Testing is still in progress regarding the development of a reliable membrane or valve to properly seal the propellant reservoir.

III. Experimental Characterization of Thrust

The prototype thruster discussed above was tested in the ASPEN Lab to demonstrate successful propellant ionization and thrust using sublimated propellant. These tests were able to successfully demonstrate plasma production within the thruster and demonstrate a net increase in thrust beyond that generated by the cold sublimation of propellant.

A. Introduction to the experimental setup used to characterize thrust

Fig. 3 illustrates a simple diagram of the current experimental setup to characterize thrust indirectly.

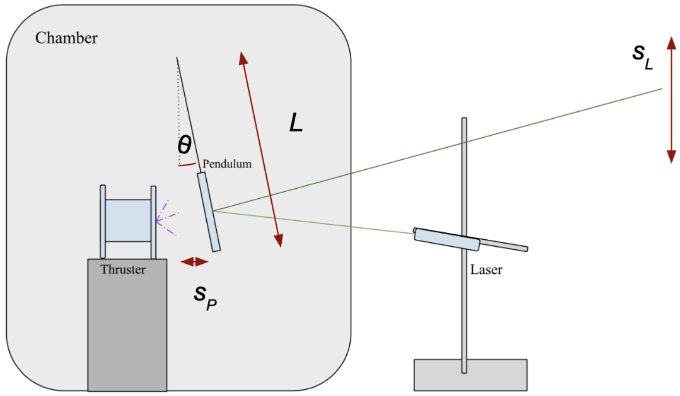

Figure 3. Diagram of the experimental setup. A laser is bounced off of a reflective pendulum to magnify its displacement for measurement.

The thrust was measured using a simple pendulum setup, where a lightweight reflective panel was secured in front of the orifice. During ionization, the pendulum moved due to the generated thrust. A laser positioned outside the chamber was used to bounce off the reflective panel, converting the horizontal movement from thrust into vertical displacement along a wall. This displacement was then translated into measurable thrust. The experiment was conducted both with and without propellant to account for and subtract the natural attraction of the pendulum to the thruster, ensuring accurate thrust measurements.

B. Details of the experimental setup

Inside the chamber, the thruster prototype was mounted onto a metal plate shielded with a layer of Kapton tape. The anode and cathode wires were connected to the probe (See Fig. 4). Suspended from metal tubing from the top of the vacuum chamber, an aluminum pendulum was placed 1 millimeter in front of the thruster orifice. The pendulum was grounded to the vacuum chamber through the metal wire that suspended it and the metal tubing's connection to the vacuum chamber body. A laser was set up outside of the vacuum chamber and directed towards the hanging pendulum such that the laser light would be reflected by the pendulum towards a vertical surface. This enables the horizontal movement of the pendulum to be transformed into vertical movement of the laser's reflected image. First, to inform how displacement correlated with thrust, the pendulum was calibrated with a micrometer. From this calibration, it was determined that every inch of laser displacement corresponded to a pendulum displacement of 0.55 millimeters. This vertical displacement was then measured through a process in which the thruster's voltage was ramped up until plasma sparked, the thruster operated for 50 seconds, and then the voltage was ramped down.

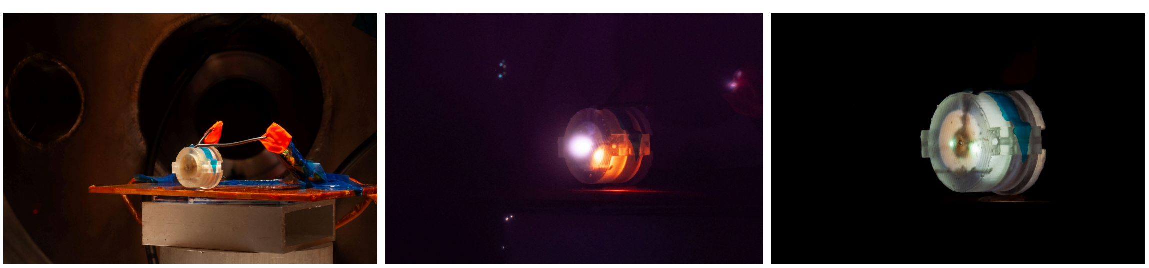

Figure 4. Thruster setup: With thruster off (Left) With adamantane flow at ~30mTorr (Center) With adamantane float ~5*10^5 Torr (Right).

C. Presentation and analysis of experimental results

The continuous oscillations of the pendulum were confirmed to be vibrations from the vacuum pumps exciting the pendulum's natural frequency of 1.09 Hz. Vibrations from the active vacuum pump were found to create these natural oscillations, with the low-pressure environment preventing damping. These oscillations are further excited by the opposing forces of thrust and electrostatic attraction between the grounded pendulum and the thruster's cathode. Displacement measurements from the pendulum were plotted over time in Fig. 5, along with a moving average with an interval of 4.17 s.

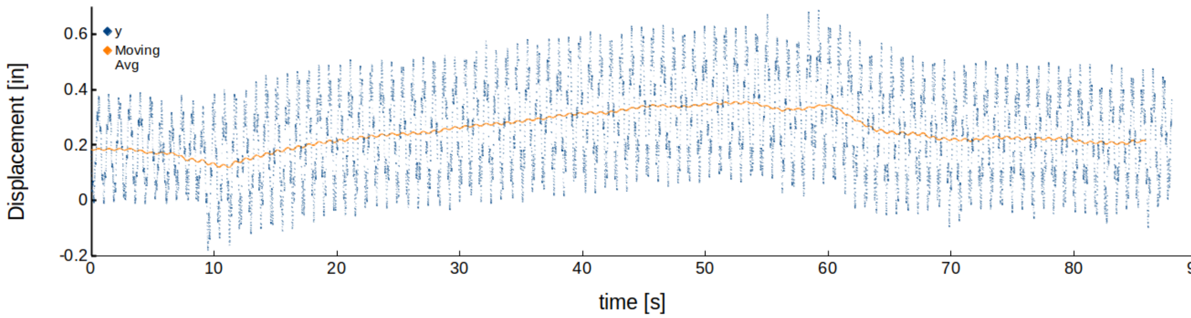

Figure 5. Raw displacement measurements with moving average (4.17 s or 1000 data point intervals). Oscillation at the pendulum's natural frequency is amplified by thrust and electrostatic attraction. Initial displacement is caused by a sublimated propellant escaping the thruster orifice, followed by a dip upon application of voltage to the thruster.

Once vertical displacement data was collected, thrust and displacement were related by

$$F_T = \frac{mgs_L C}{L} \tag{1}$$

Where F_T represents thrust in newtons, m represents pendulum mass in kg, s_L is the vertical displacement along the wall in inches, C is 5.5×10^{-4}, and L is the length of the pendulum in meters. A moving average is used to determine thrust in order to compensate for the oscillatory behavior previously described. Further correction was also performed to account for the electrostatic effects, which were measured to be a nearly constant -1 µN. Fig. 6 shows the resulting thrust profile along with real-time power, voltage, and current data.

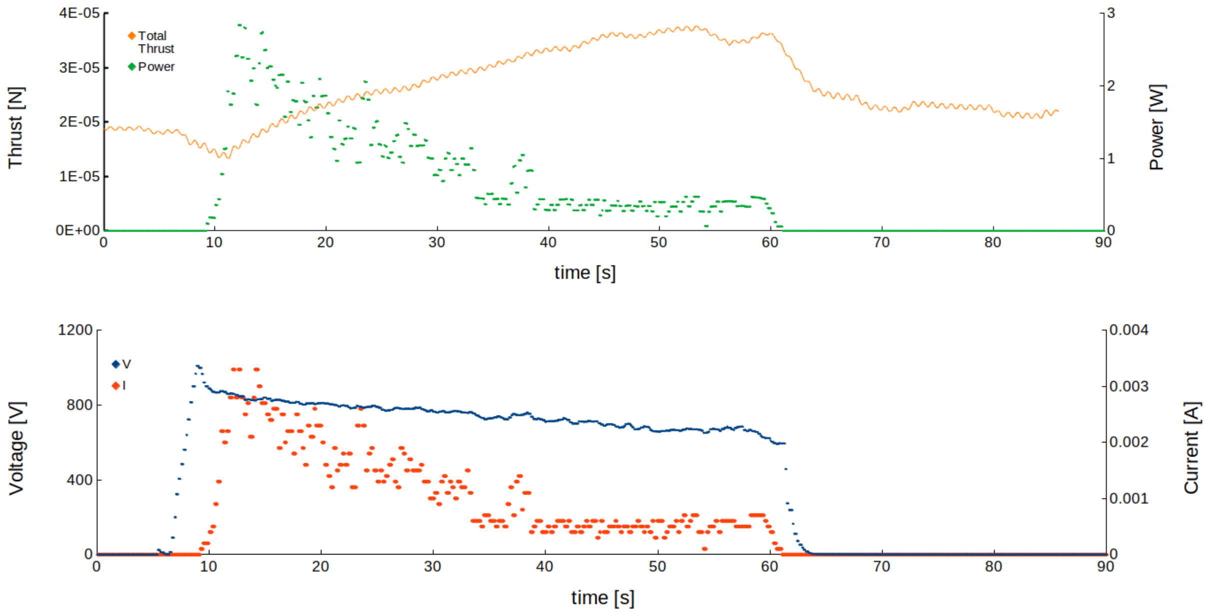

Figure 6. Thrust power measurements (top) with corresponding voltage and current measurements (bottom). The approximately 2-second delay in the onset of current suggests that the initial displacement is due to electrostatic attraction.

When operating at full power using propellant, the average thrust value was calculated at 29 µN, in comparison to 18 µN when operating unpowered and in a cold gas mode. Analysis of power consumption found the thruster to have an average thrust efficiency of 100 µN per watt, with a minimum efficiency of 10 µN per watt. The proof-of-concept thruster has shown that thrust can be generated using ionized adamantane as a solid propellant. Additionally, these thruster tests allowed for the build-up of ASPEN's electric propulsion testing hardware. The next phase of thruster development will be the optimization of thrust and efficiency performance by comparing iterated experimental results with an ongoing simulation effort. To increase the precision of thrust measurements, ASPEN is currently constructing an inverted pendulum thrust stand to capture direct thrust measurements.

IV. Experimental Characterization of Plasma Environment

A. Details of the experimental setup

Currently, the ASPEN lab is developing capabilities to test electric propulsion devices beyond thrust characterization. Another important aspect of the thruster to consider is the plasma environment it creates while firing, which can offer key insights into how the thruster interacts with the area around it.

To characterize the environment surrounding an older iteration of the thruster during operation, we designed and constructed a Langmuir probe. Influenced by a design described by Li et al.,[7] the probe itself consists of a ~6mm diameter circular tantalum sheet spot welded to Teflon-coated wire. The wire is supported structurally with three PVC-coated wires and is insulated by polyolefin shrink wrap and a layer of polyamide (Kapton) tape. The probe is connected to a data collection circuit outside the vacuum chamber via a feedthrough flange. A bias voltage, V_{bias} (V_B in Fig. 6), modulated by a 100mHz waveform generator and amplified by an op-amp, is recorded through a digital oscilloscope. An analog I/O DAQ device, linked to LabView, records the voltage, $V_{R,}$ across a 10 kΩ resistor.

Two different types of plasma were analyzed: plasma created with ambient air and adamantane plasma. To characterize the plasma of rough-vacuum air, only ambient air was introduced into the thruster through a feedthrough system. For adamantane plasma, the same procedure was done with the addition of approximately 0.3

grams of the compound into the feedthrough system and resultantly the thruster. This testing was conducted under rough vacuum conditions, maintaining chamber pressure at 120 ± 5 mTorr, and the thruster was powered with a voltage of approximately 1.8 kV.

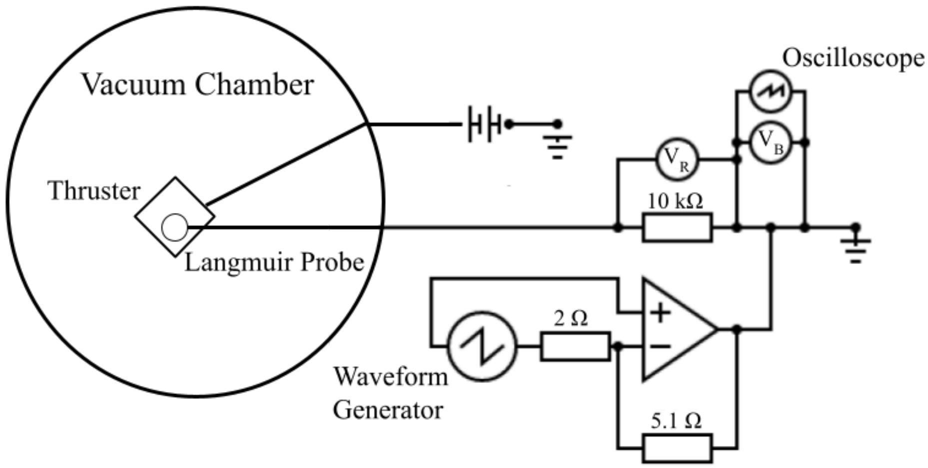

Figure 6. The Langmuir probe and associated data collection circuit setup.

B. Presentation and analysis of preliminary experimental results

To characterize this prior iteration of the thruster, five individual sweeps of the probe were isolated from the data for both the ambient plasma and adamantane plasma configurations and processed. The collected data for the voltage supplied by the waveform generator, V_{bias}, were recorded in volts and the voltage across the 10 kΩ resistor, V_R, was recorded in millivolts. V_R data were converted to current using the relation $V_R R = I$ where R = 10 kΩ. The current I and voltage V_{bias} were plotted to form an I-V curve to describe the environment around the thruster.

After data acquisition, it was observed that the data collected by LabView contained noise, mainly observed in data clustered around the ion saturation current throughout the I-V trace. These data were filtered out, however they warrant further investigation in the future to improve probe accuracy. After analyzing the processed data, values for different plasma properties were calculated for each of the five sweeps.[8] The standard deviation of the values was found and the data analyzed are summarized in Table 1, with the percent error calculated at one standard deviation for each property.

Property	Ambient Plasma	Propellant Flow
Electron density (n_e), m^{-3}	$4.17 \times 10^{17} \pm 10.9\%$	$5.79 \times 10^{17} \pm 11.9\%$
Electron temperature (T_e), eV	$2.90 \pm 22.0\%$	$5.68 \pm 18.1\%$
Plasma potential (Φ_p), V	$12.63 \pm 2.3\%$	$12.32 \pm 5.1\%$
Floating potential (Φ_f), V	$9.90 \pm 6.4\%$	$5.39 \pm 30.5\%$

Table 1. Properties for ambient plasma and propellant flow from automated data collection.

These preliminary results support the use of adamantane as a fuel, indicating that the plasma environment of the propellant flow has a higher electron density and temperature, contributing to more thrust. However, these results should be viewed with caution. This system is still in development, and simplifying assumptions were made in the data collection process. Future work includes refining the Langmuir probe design, enhancing data collection and analysis methods, and constructing additional probes, such as Faraday probes, to improve confidence in results and enable more accurate analysis of additional characteristics. As the thruster's design continues to iterate, using in-house constructed plasma diagnostics methods will provide an economic and reliable method to gain insight into the environment around the thruster. This information will be critical to capture inefficiencies in thruster design to allow improvements to specific impulse and thrust values.

V. Numerical Analysis

The experimental effort was supplemented with a numerical analysis. Two sets of numerical studies were performed: parametric studies of discharge plasma dynamics and molecular dynamics studies of propellant fragmentation. These two models are described below.

A. 2D plasma simulations

Two-dimensional plasma simulations were performed using the two-dimensional open-source general-purpose plasma and rarefied gas code Starfish.[9] The computational domain is shown in Fig. 7. The simulation used a 160x66 node Cartesian mesh with uniform cell spacing of 0.1 mm. The simulation started with a neutrals-only run in which neutral adamantane molecules were loaded into the propellant tank section with a density corresponding approximately to 0.02 kPa vapor pressure.[10] These molecules, as well as all species used in the simulation, were represented using simulation particles. The molecules were then allowed to expand by simulating 10,000 10-8 s time steps. The produced neutral density is seen in Figure 8.

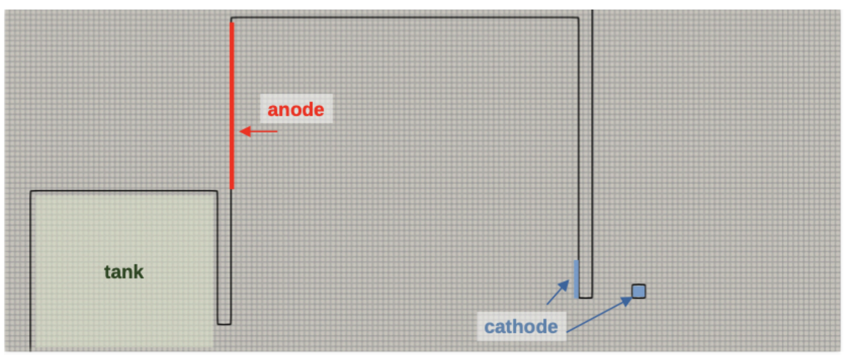

Figure 7. Computational Domain

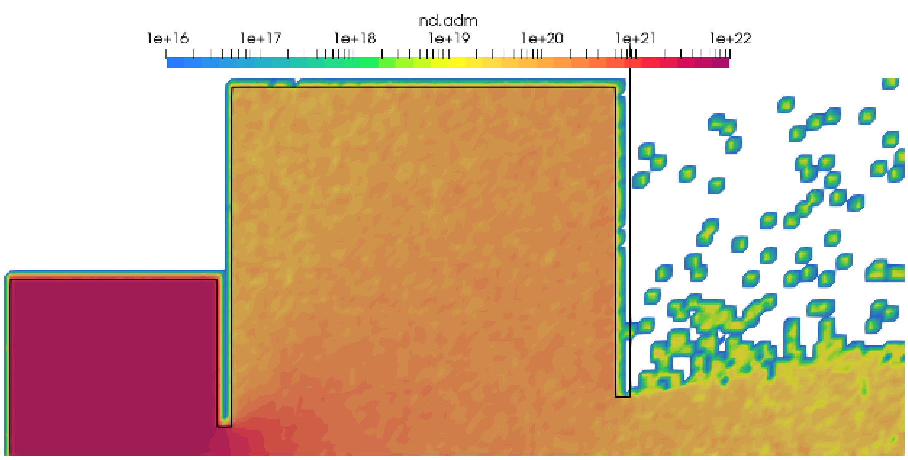

Figure 8. Initial neutral density

The simulation was subsequently restarted with this initial neutral particle population and was nominally run for 100,000 10-12 second time steps. The simulation utilized the Electrostatic Particle inCell (ES-PIC) method. As will be noted below, some runs were terminated earlier, since all simulations were found to reach an oscillatory steady state after around 40,000 time steps. A much smaller time step was needed in these runs to resolve electron dynamics. Electrons were sampled from the cathode surface with counts corresponding to 2 mA of current. The potential on the cathode was fixed at - 20 V while the anode surface was set to 2000 V. Plasma potential was obtained by solving the linear Poisson's equation, using the Gauss-Seidel method. An electric field was used to accelerate plasma particles according to the Lorentz force. The electrons, born with an initial thermal velocity corresponding to 500 K, accelerate rapidly in the electric field imposed by the two electrodes. Ionization was modeled using the Monte Carlo Collisions (MCC) method, with probability given by where the terms in the parentheses correspond to the collision cross-section, neutral density, relative velocity, and the time step, respectively. The ionization cross-section was based on a tabulated form of data from.[11] One particular challenge involved in modeling ionization using particle-based approaches is that initially a small macro particle weight is needed to produce a statistically sufficient number of particles for the process to begin. However, once ionization begins, such tiny particles will quickly overwhelm the available computational resources. Therefore, every two-time steps, smaller weight particles were merged into larger ones using a moment-conserving scheme outlined by Fox.[12]

The simulations were used to compare several different configurations. These configurations primarily affected the location of the anode. However, we also compared the effect of an external cathode. Fig. 9 compares the electron densities for the nominal configuration (left) to the one containing the external hot-wire filament (right). The second configuration is primarily seen to yield higher electron densities in the external region, which may be desired for plume neutralization purposes. This configuration also suggests a higher electron population at the exit orifice which may be beneficial for overcoming ion extraction charge saturation limits.

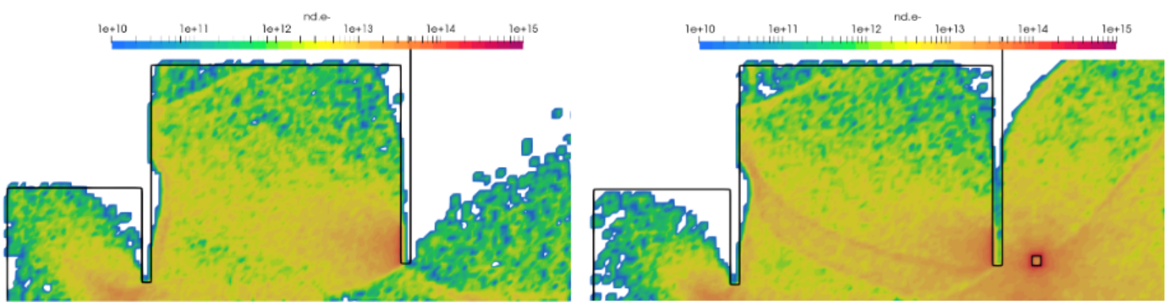

Figure 9. Electron density without (left) and with (right) external electron source

Fig. 9 visualizes the evolution of ion density using the nominal configuration which corresponds to the sketch in Fig. 6. The snapshots correspond to 10,000, 28,500, 32,000, and 40,000 time steps. The evolution of plasma potential corresponding to these same steps is plotted in Fig. 10. The ion density remains essentially in the state seen in the final figure for the remainder of the simulation run. We can observe that initially, ions form in the vicinity of the anode, as expected, given that this is the region where electrons have the highest kinetic energy. Subsequently plasma "arc-like" formation forms. While leading to the desired axial electric field, it also allows electrons to expand into the propellant tank section. The high vapor pressure of the adamantane found here leads to the formation of dense plasma at around 1019 (#/m3) number densities. Resolving the Debye length here would require a finer computational mesh, in the absence of which, the Poisson solver has difficulties converging, leading to non-physical high (>50 kV) plasma potentials. The simulations will be re-run as part of future work with localized mesh refinement in this region. However, despite the large value of potential, the simulation does not "blow up", and instead predicts a steady state configuration as shown by the last ion density plot and also by the time-averaged plot in Fig. 11. It is speculated that the roughly two orders of magnitude decrease in ion density from the thruster interior to the plume is due to the Child-Langmuir charge saturation limit.

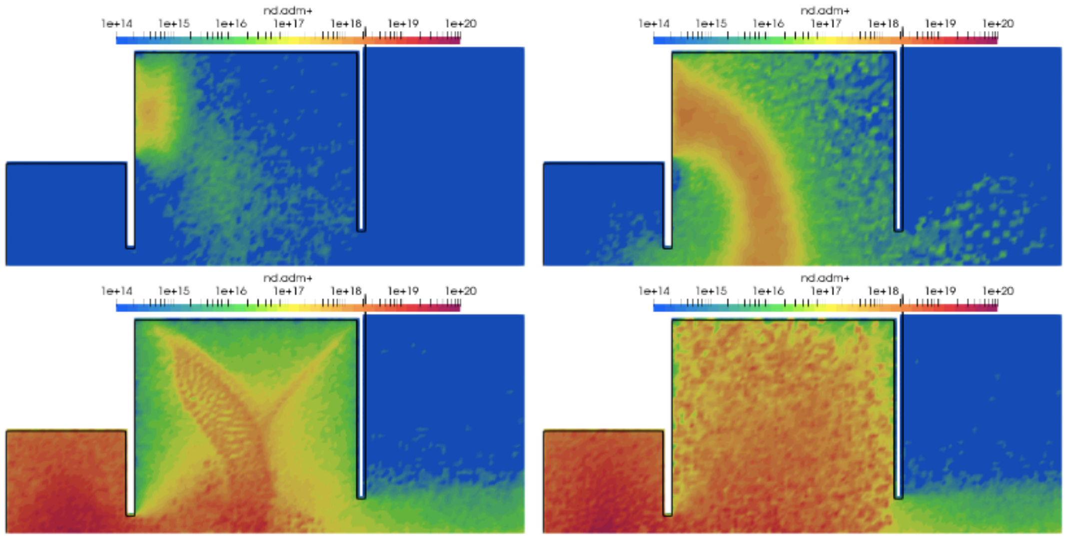

Figure 10. Ion density after (a) 10,000, (b) 28,500, (c) 32,000, and (d) 40,000 time steps.

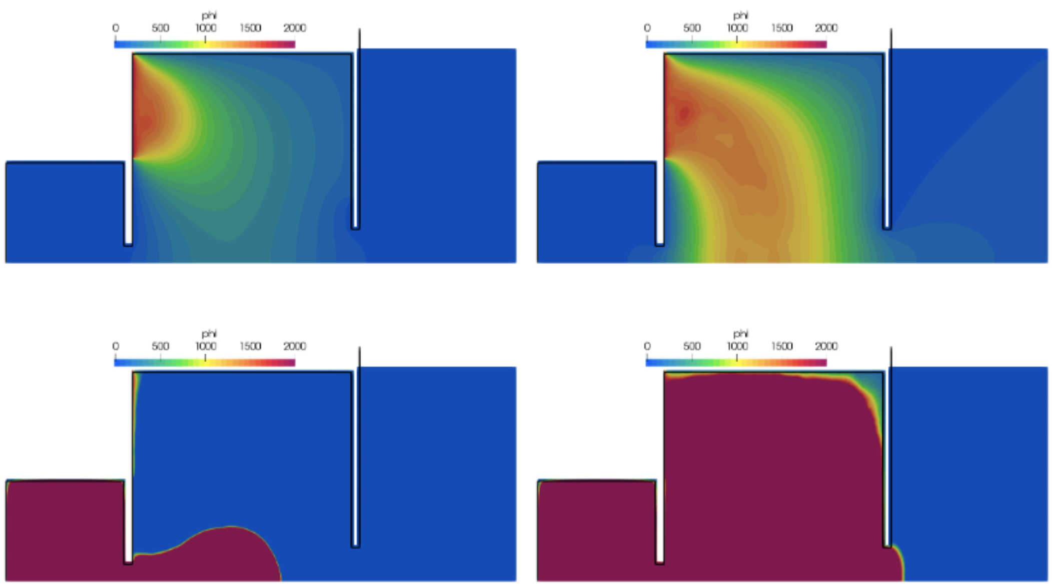

Figure 11. Evolution of plasma potential at time steps corresponding to the prior figure. The potential solver produces non-physical potentials once dense plasma forms in the propellant tank.

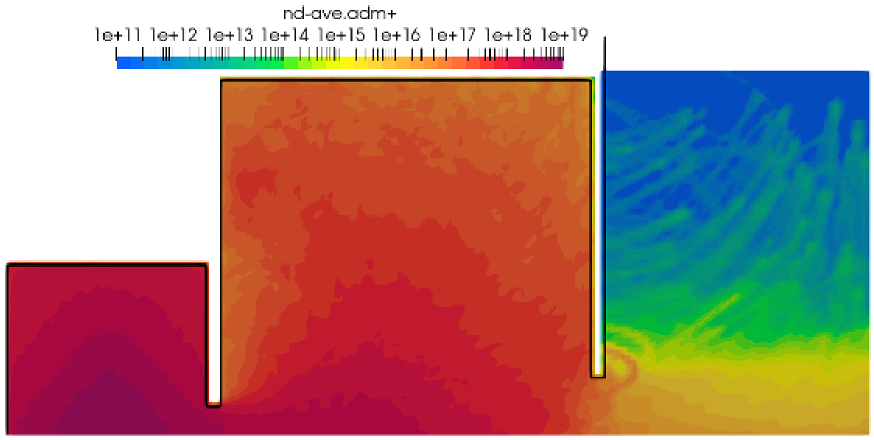

Figure 12. Time-averaged ion density

Fig. 12 next plots the time evolution of ion density for the run with the external cathode. While some difference in the initial electron densities was apparent in Fig. 8, we do not observe any noticeable impact on the ion population or the extracted plume profile once the dense plasma forms inside the thruster discharge chamber.

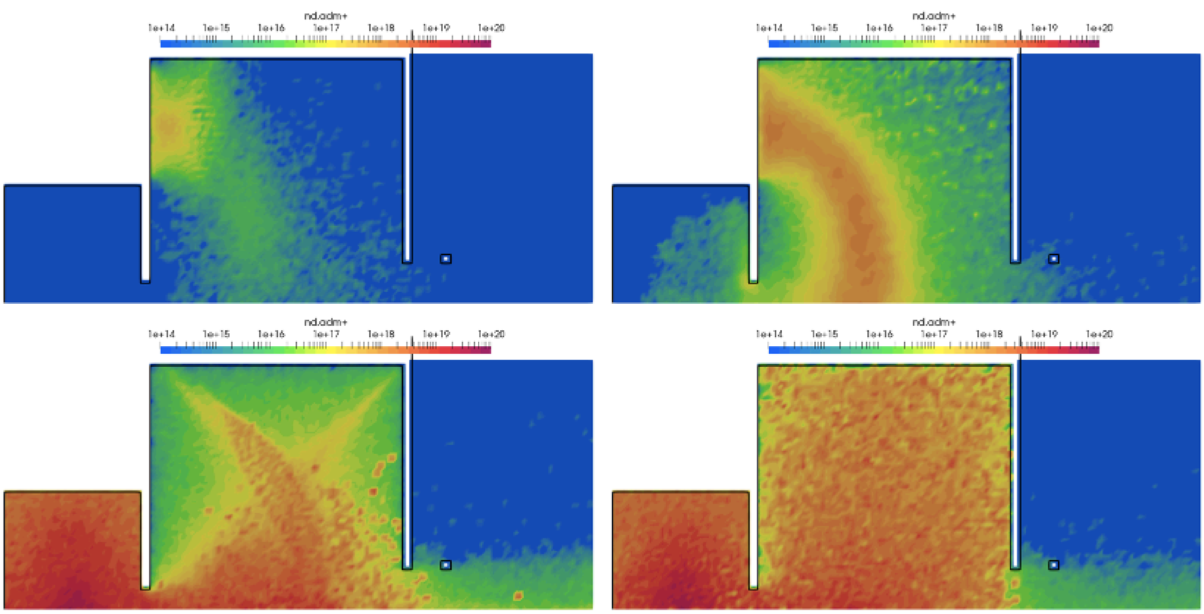

Figure 13. Evolution of ion density with external wire emitter, time steps 10,000, 21,500, 26,500, and 40,500.

We have also considered several alternate thruster configurations. One of these was the "back anode", in which the anode was placed at the back of the propellant tank. Snapshots of ion density from this run are shown in Fig. 13. Note that while the actual time steps differ from Fig. 9 due to the different temporal responses in all configurations, we attempted to capture approximately the same events. We can see that with the back anode, ionization begins in the propellant tank, as expected. Once ionization starts, we obtain a steady state comparable to the nominal configuration.

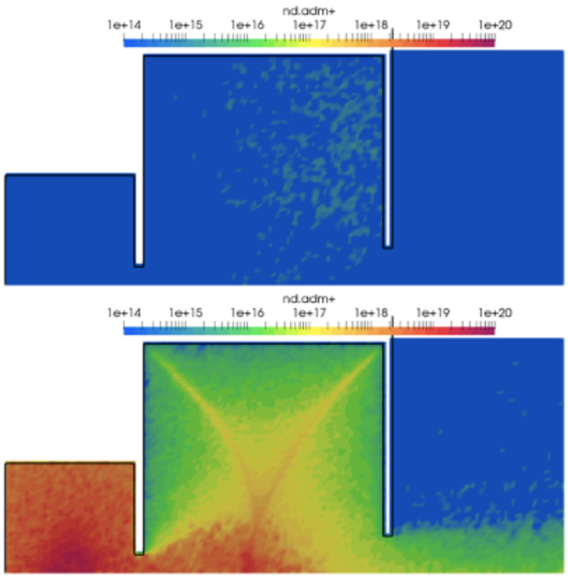

Figure 14. Evolution of ion density with “back anode”. Snapshots correspond to time steps 10,000, 15,500, 17,500, and 81,000

Fig. 14 then plots ion density for a “big anode”, in which the entire back wall separating the discharge region from the propellant tank acted as the anode. Fig. 14 shows results from a run with a conical discharge chamber. While again the initial plasma formation is different, all configurations eventually lead to the formation of dense plasma inside the propellant tank. As part of our future work, we will investigate this “ignition” process in more detail by utilizing a finer computational mesh and smaller simulation time steps to improve the capture of electron dynamics. Subsequently, we will use numerical simulations to study alternate extractor designs to increase the current density of the emitted plume.

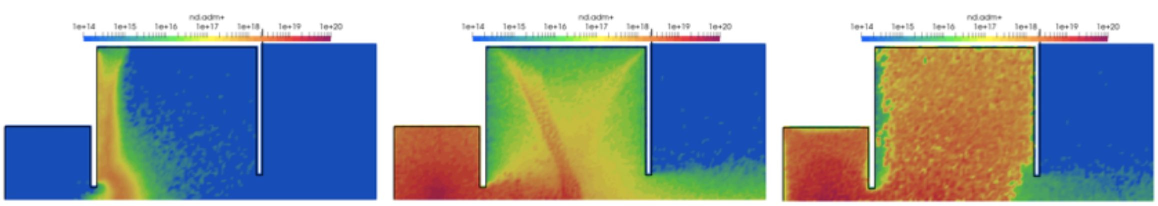

Figure 15. Evolution of ion density with “big anode” at time steps 6,000, 9,000, and 70,000

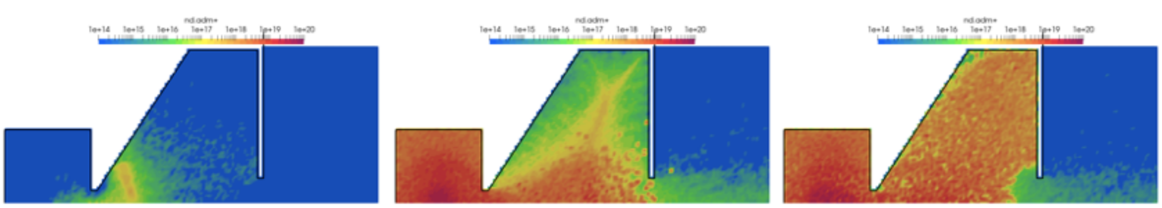

Figure 16. Evolution of ion density with “triangular cone” at time steps 10,000, 65,500, and 79,500

B. Molecular dynamics simulations

Molecular dynamics simulations were conducted using the free and open-source program LAMMPS (Large-scale Atomic/Molecular Massively Parallel Simulator) with reaxFF (Reactive Force Field), a bond-order-based force field. ReaxFF has applications in molecular dynamics and specifically provides information on bond breaking and formation. Units are in real units, so the domain is an 80 Å x 80 Å x 80 Å cube shown in Fig. 17.

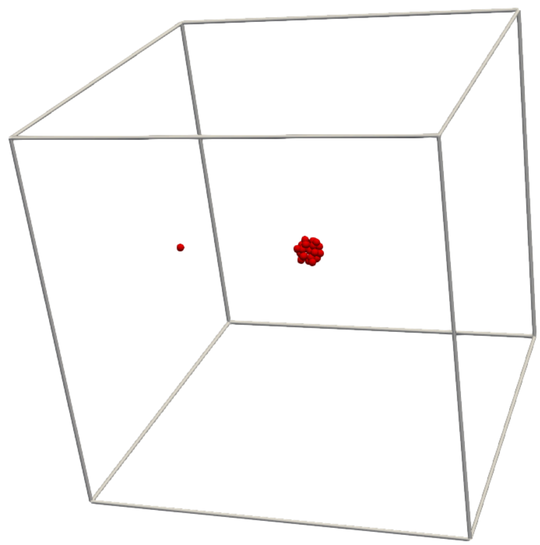

Figure 17. Molecular Dynamics Simulation

Through the reaxFF force field, carbon and hydrogen atoms are defined in the simulation as single-atom types. Temperature is initialized at approximately 300 K, and conducted in the NVE ensemble which conserves the total energy through the collision as opposed to fixing the temperature. Within reaxFF, which specifies the forces between the atoms, it was specified that the adamantane molecule has internal energy, while the incident particle (hydrogen, in this case) is treated as a kinetic particle with velocity 0.5 in real units (50,000 m/s) so it has no incident energy. This is an approximation of an electron colliding with an adamantane molecule and velocities scaled to that of an electron.

The University of Southern California's Center for Advanced Research Computing (CARC) was utilized, where a minimal simulation with a hydrogen atom as an incident particle was set up. Submitted jobs to CARC would then run the simulation for a total of 2000 time steps, each time step 0.1 in real units, which corresponds to approximately 0.1 femtoseconds, and a total run time of 0.1 picoseconds. CARC simulations returned data files that included the number of species, as well as the types of species that each simulated collision produced. From the input files, the energy levels of the adamantane were varied by adjusting its velocity. Table 2 contains the input data (Energy and Hydrogen Velocity) and the outputs, the produced species types. An additional run where a moving adamantane molecule collides with a stationary adamantane molecule is included in Table 3. Although not the focus of this simulation, it provides some additional information on a likely event within the thruster.

Data visualization for Fig. 19 and Fig. 20 is using Paraview, an open-source multiple-platform application for animating the collision process. These images show some examples of the changing atom arrangements as simulated ionization occurs. For Fig. 21, 22, and 23, an open-source Java viewer for chemical structures, called Jmol, is used to illustrate the bond structures.

Table 2. Single hydrogen colliding with stationary adamantane.

Energy (real)	**Hydrogen Velocity (real)**	**# of Species**	**Species Types**
275	0.5	1	C10H16
285	0.5	1	C10H16
290	0.5	2, 1	C9H14, CH2, C10H17
295	0.5	2	C7H11, C3H5
298	0.5	2	C10H16
300	0.5	2,1	C8H13, C2H3, C10H17
301	0.5	1	C10H16
305	0.5	1	C10H16
300	0.45	2, 1	C10H15, H, C9H14, CH2 C10H16, C10H17
300	0.25	1	C10H16
300	0.30	1	C10H16

Table 3: Adamantane colliding with stationary adamantane.

Energy (real)	Incident Adamantane Velocity (real)	# of Species	Species Types
300	0.5	5	C2, C, CH, H, H2

In Fig. 18 and Fig. 19, the orientation angle of the visualization is held constant, and the arrangement of the atoms within the molecule at a molecule velocity of 295 shows clear fragmentation. From the output files generated by the simulation, at the end of the run, there are two species instead of the initial one. Although not explicitly shown in the visualization, the output files show that C7H11 and C3H5 are generated.

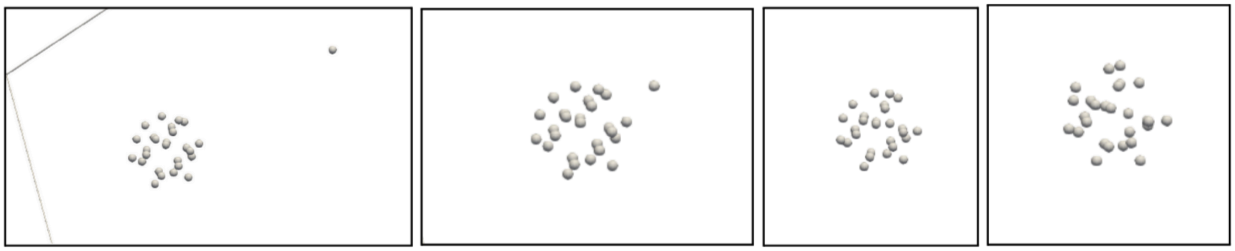

Figure 18. For a molecule velocity of 295, atom arrangement at time steps 300, 500, 600, 700.

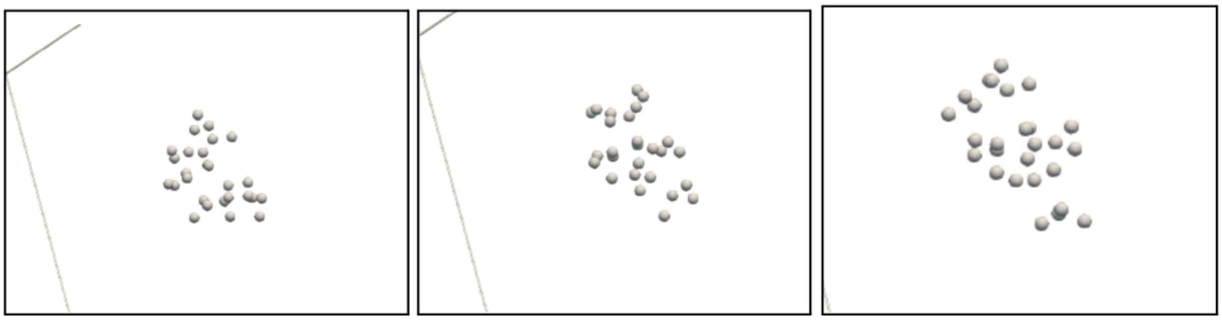

Figure 19. For a molecule velocity of 295, atom arrangement at time steps 1000, 1500, 2000.

However, as shown in Fig. 20, 21, and 22, we see that the hydrogen atom bonds with the adamantane molecule instead of being treated as a kinetic particle, illustrating that the hydrogen still has some lingering chemical properties. Ideally, the hydrogen atom would have no other energy aside from its kinetic energy and perhaps some Coulomb energy if it were to approximate an electron. However, in this simulation, the incident hydrogen atom was treated no differently than any of the other adamantane hydrogens, except it had a very high initial velocity relative to the adamantane. When approaching the adamantane, some chemical potential energy is exchanged, meaning the assumption of a simple kinetic particle breaks down at this point.

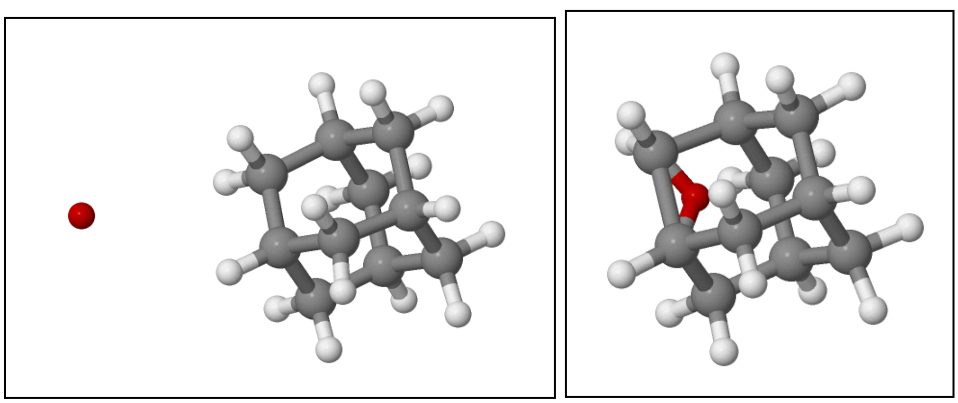

Figure 20. For a molecule velocity of 300, atom arrangement at time steps 500, 600.

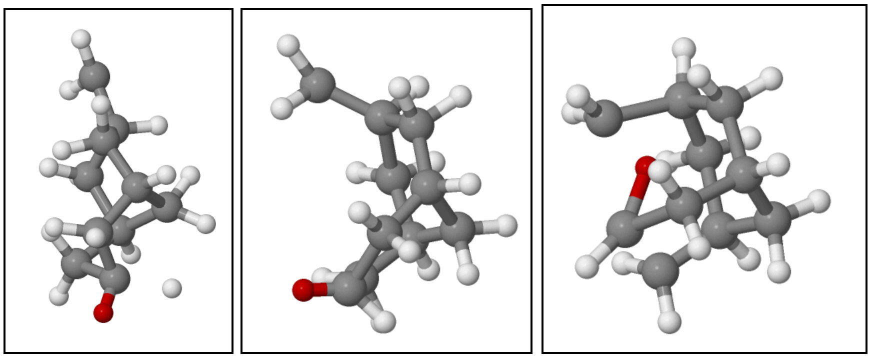

Figure 21. For a molecule velocity of 300, atom arrangement at time steps 700, 1000, 1500. Incident hydrogen is in red.

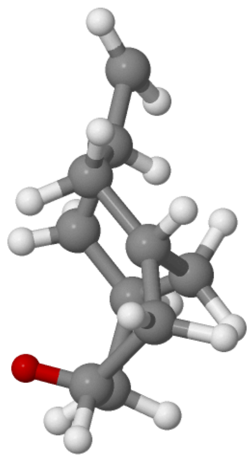

Figure 22. For a molecule velocity of 300, the final configuration at time step 2000. This is a C10H17 molecule.

In future simulations, slightly higher velocities would be preferred so that the incident hydrogen atom leaves the system after the collision, even if it results in a higher collision energy than initially intended. It would also be likely the functional form would need to be reworked so that the incident hydrogen will not react aside from exchanging kinetic energy with Coulombic energy. Furthermore, additional simulations would likely rely on a greater number of runs to generate a better statistical model for the species generated from hydrogen-adamantane collisions. Additionally, given more time, an electron-adamantane model would more accurately describe the situation but would require greater setup. Electrical interactions could also be taken into consideration.

VI. Conclusion

A. Summary of the development and characterization of the adamantane thruster

Over the past year, ASPEN has designed and constructed a proof of concept ion thruster using solid adamantane as a propellant with a focus on implementation in the deorbiting mechanisms of CubeSats. A prototype thruster was 3D printed from a clear resin and tested under vacuum using a pendulum thrust stand. A thrust value of 29 µN was obtained**.** Plasma simulations guided the thruster design and were supported by the construction of a Langmuir probe to characterize the plasma environment within the thruster bloom. High electron density and temperature were found, again indicating favorable properties to generate thrust. Molecular dynamics simulations produced evidence that a collision between an adamantane molecule and a kinetic particle, with energy corresponding to the thermal electrons of interest in the system, can indeed result in carbon-carbon bond scission which destabilizes the adamantane. If operating under comparable ISP values to conventional CubeSat deorbiting mechanisms, it was found that solid adamantane propellant promises a significant reduction in the mass and volume of fuel needed. Additionally, due to the single-use nature of the proposed thruster, complex pressurization equipment is no longer necessary, further reducing the mass of such a device in comparison to industry-standard devices. During the development of a single-use thrust containment method for the adamantane propellant, ASPEN focused on constructing a membrane that could be removed or broken upon firing of the thruster. Several potential membrane materials were tested with inconclusive results requiring further investigation.

B. Reflections on the research outcomes and areas for future investigation

As a student organization, ASPEN is proud of the current progress made in developing a plasma testing facility and related equipment. Our immediate goal is to expand our testing capabilities by including an inverse pendulum thrust stand. This addition will enable us to obtain more direct and accurate thrust measurements, enhancing the reliability and accuracy of our data. Furthermore, we aim to continue refining our thruster to improve its producibility and functionality, including the incorporation of a working membrane or valve to enclose our adamantane reservoir. Finally, we hope to continue expanding our ability to characterize our plasma. A Faraday Probe and Residual Gas Analyzer will further our understanding and help to improve our simulation capabilities.

ASPEN hopes to partner with the USC Space Engineering Research Center (SERC) to develop a comprehensive propulsion system. This collaboration aims to integrate our propulsion technology onto one of SERC's 3U CubeSats, providing real-world application and validation. Before this deployment, more efforts will need to be made to develop a power control system to ensure our system can be properly operated within the confines of a CubeSat and adjustments will need to be made to the thruster body to ensure it is flight ready.

Acknowledgments

The authors would like to thank the members of the ASPEN Lab at the University of Southern California. The combined efforts of the lab members have been essential in the development of the thruster. The authors thank the University of Southern California's Viterbi School of Engineering for its generous support, as well as Northrop Grumman, Blue Origin, and Boeing for their sponsorship of the lab. We hope to continue our research and help the next generation of engineers gain skills with their continued support.

References

[1]K. Lemmer, "Propulsion for CubeSats," *Progress in Aerospace Sciences*, vol. 74, pp. 1-15, January 2015. Available: https://www.sciencedirect.com/science/article/pii/S0094576516308840

[2]M. M. Micci and A. D. Gallimore, "Micropropulsion for Small Spacecraft," *Proceedings of the 34th International Electric Propulsion Conference*, IEPC-2015-364, October 2015. Available: https://pepl.engin.umich.edu/pdf/IEPC-2015-364.pdf

[3]R. Q. Dunn et al. "MiPS Standard, Rev. 0714." VACCO Industries, July 2014, https://www.vacco.com/images/uploads/pdfs/MiPS_standard_0714.pdf

[4]A. Mehrparvar et al. "CubeSat Design Specification Rev. 13." California Polytechnic State University, February 2014, http://static1.squarespace.com/static/5418c831e4b0fa4ecac1bacd/t/56e9b62337013b6c063a655a/1458157095454/cds_rev13_final2.pdf

[5]J. Russell and N. Kilkenny. "ALBus hopes to increase power availability for CubeSats." NASA, December 2018, https://www.nasa.gov/general/albus-hopes-to-increase-power-availability-for-cubesats/

[6]Benchmark Space Systems. "BSS Starling Datasheet 20-2." Orbital Transports, 2020, https://catalog.orbitaltransports.com/content/brands/benchmark/BSS%20Starling%20Datasheet%2020-2.pdf

[7]Li, P., Hershkowitz, N., Severn, G. "Building Langmuir Probes and Emissive Probes for Plasma Potential Measurements in Low Pressure, Low Temperature Plasmas." J. Vis. Exp. (171), e61804, https://doi.org/10.3791/61804 (2021)

[8]Merlino, R. L. (2007). “Understanding Langmuir probe current-voltage characteristics.” American Journal of Physics, 75(12), 1078–1085. https://doi.org/10.1119/1.2772282

[9]Brieda, L., and Keidar, M., “Development of the Starfish plasma simulation code and update on multiscale modeling of Hall thrusters”, *48th AIAA Joint Propulsion Conference*, Atlanta, GA, 2012

[10]Mokbel, I., Ruzicka, K., Majer, V., Ruzicka, V., Ribeiro, M., Jose, J., and Zabransky, M., “Vapor pressures and thermal data for three high-boiling compounds of petroleum interest: 1-phenyldodecane, (5 alpha)-cholestane, adamantane”, *Fluid Phase Equilibria*, Vol. 169, pp. 191-207, 2000

[11]Tsipinyuk, B., Bekkerman, A, Kolodney, E. “Binary encounter models for electron ionization of atoms: A one parameter expression for electron energy dependent (E < 200 eV) single ionization cross section”, *International Journal of Mass Spectrometry,* Vol. 2, No. 16, pp. 328–329, 2012

[12]Fox, J., *Advances in Fully-Kinetic PIC Simulations of a Near-Vacuum Hall Thruster and Other Plasma Systems*, Ph.D. Dissertation, Department of Aeronautics and Astronautics, Massachusetts Institute of Technology, 2007